This article has been accepted for publication in a future issue of this journal, but has not been fully edited. Content may change prior to final publication. Citation information: DOI 10.1109/TVT.2016.2574740, IEEE Transactions on Vehicular Technology

Fuel-saving Servo-Loop Control for Adaptive Cruise Control System of Road Vehicles with Step-Gear Transmission

Shengbo Eben Li, *Member, IEEE*, Qiangqiang Guo, Long Xin, Bo Cheng, Keqiang Li

***Abstract*—Fuel consumption of fossil-based road vehicles is significantly affected by the way vehicles are driven by drivers. The same is true for automated vehicles with longitudinal control. This paper presents a periodic servo-loop longitudinal control algorithm for adaptive cruise control (ACC) system to minimize the fuel consumption in car-following scenarios. The fuel-saving mechanism of pulse-and-glide (PnG) operation is first discussed for the powertrain with internal combustion engine and step-gear transmission. The servo-loop controller is then designed based on a periodic switching map for the real-time implementation, and adjusted with a range-bounded feedback regulator to enhance the robustness to model mismatch. Simulations in both uniform and natural traffic flows demonstrate that this algorithm achieves significant fuel saving benefit in automated car-following scenarios up to 8.9% in naturalistic traffic flow (when coasting at neutral gear) compared to a linear quadratic (LQ) controller. Meanwhile, its inter-vehicle range is preferably bounded so that the negative impact on safety and traffic smoothness is contained.**

***Index Terms*—Automated vehicle, eco-driving, adaptive cruise control, car-following, fuel economy.**

I. Introduction

NOWADAYS, road vehicles mostly count on petroleum-based fossil fuel which causes a lot of problems such as energy shortage and environmental pollution [1], [2]. As is revealed by former studies, fuel consumption of road vehicles is influenced by factors like vehicle design, road infrastructure as well as driver behaviors [3]. Many advanced techniques such as lightweight and hybridization have been applied to reduce the fuel consumption over the last decades [4], [5], [6], [7], [8], [9]. Recently, the relationship between fuel economy and driver behavior has been attracting increasing attention. For example, Boriboonsomsin *et al.* (2010) find that the fuel economy on city streets improves by 6% on average by using an instantaneous fuel economy feedback device to improve driver behavior [10]. Sivak *et al.* (2012) illustrate that driver behavior such as tactical decisions and operational decisions can contribute to about 45% reduction in fuel economy for light-duty vehicles [11]. Generally speaking, fuel-efficient driving (or called eco-driving) behaviors can save fuel from 5% to 15% [12]. Compared to conventional fuel-saving techniques which have almost reached their limit, eco-driving has a relatively high potential of reducing fuel consumption [13].

Eco-driving has been put into practice particularly in Europe and Japan, focusing on educating or guiding drivers to improve their behavior empirically [14], [15]. For example, drivers are taught to apply fuel-saving driving tips in their daily commute, i.e., avoiding frequent braking, selecting the optimal gear, maintain the economic speed, and stop idling engine at a long-waiting intersection. It is found that drivers could save fuel consumption right after education, but the fuel reduction would degrade in long-term due to the human complacency and behavioral regression [16]. To achieve long-term improvement, fuel-saving tips can be implemented in control algorithms under certain driving conditions to eliminate the negative influence of behavioral degradation and uncertainty. This paper focuses on the fuel-efficient longitudinal automated driving of road vehicles in the car-following scenarios, which is one of the most common and basic driving tasks.

There are two types of driver assistance systems to be designed to save fuel, i.e., predictive cruise control (PCC) and fuel-oriented adaptive cruise control (ACC). The traditional cruise control (CC) system often applies the constant speed (CS) policy, which means that the vehicle will run at a preset speed until the driver depresses the throttle or brake pedal. However, traditional CC will tend to over-throttle on the upgrades and retard on the downgrades, wasting the energy storage capabilities available from the inertia of the vehicle. The PCC then is proposed to overcome the disadvantages of CC by using the altitude information from a three-dimensional map. Measuring the surface slope of road ahead, the PCC allows vehicle speed to vary around the setting speed to get better fuel economy [17], [18]. Hellstrom *et al*. proposed a look-ahead controller based on the combination of road slope database and GPS unit. They use the dynamic programming algorithm to

This work was supported by the National Natural Science Foundation of China under Grant 51575293. The first two authors, i.e., S. Li and Q. Guo, contributed equally to this work. All correspondence should be sent to S. Li.

S. Eben. Li is with the State Key Laboratory of Automotive Safety and Energy, Department of Automotive Engineering, Tsinghua University, Beijing 100084, China. He was with University of California, Berkeley, as a visiting scholar, Berkeley, USA. (e-mail: lisb04@gmail.com)

Q. Guo, L. Xin, B. Cheng, K. Li are with the State Key Laboratory of Automotive Safety and Energy, Department of Automotive Engineering, Tsinghua University, Beijing 100084, China. (e-mail: {gqq14, xin-l13}@mails.tsinghua.edu.cn, {chengbo, likq}@tsinghua.edu.cn)

This article has been accepted for publication in a future issue of this journal, but has not been fully edited. Content may change prior to final publication. Citation information: DOI 10.1109/TVT.2016.2574740, IEEE Transactions on Vehicular Technology

constantly feed the controller with new speeds [19]. Different from CC, ACC automatically adjusts the vehicle speed to maintain a safe distance from a target vehicle ahead, which impedes the accelerating and braking behavior of ego vehicle in the form of kinematic constraint. Nowadays there are three main strategies used in the design of fuel economy oriented ACC: (1) Shortening inter-vehicle distance [21]; (2) Cooperative control of engine and powertrain [20]; (3) Smoothing longitudinal acceleration [22]. The first strategy can be effective due to the lower aerodynamic drag when the inter-vehicle distance is shortened. The second strategy aims to increase the probability of engines working in the economic region to reduce fuel consumption. The third strategy reduces acceleration level to decrease the extra loss of energy. Although useful in theory, these three strategies have disadvantages when applied to real vehicles: The first strategy has relatively high risks of rear-end collision; the second strategy is limited by the high cooperative complexity; and the third strategy is limited only dynamic traffic and becomes less effective in smooth scenarios. Moreover, their fuel benefit is quite limited because most of them are statistically concluded from driver experiment data. Regarding fuel optimal operation, Li and Peng (2012) has found that in car-following scenarios, the pulse-and-glide (PnG) operation performs the best in fuel economy for road vehicles with continuous variable transmission (CVT) [23], [24]. The PnG uses a periodic operation, which runs the engine at the most efficient point to accelerate and then coasts down to a lower speed. The key of PnG process is to store and release inertial energy efficiently by periodic operation. To achieve the application of PnG, the operation points of engine and the ratios of CVT must be controlled periodically and accurately, which is rather challenging [25]. Further work executed by Li *et al.* focuses on a servo-loop PnG controller for vehicles with CVT and they find that it can reduce fuel consumption significantly [26]. The similar effect is found on traffic flow for a platoon of mixed automated and manually driven vehicles [27]. Unlike the one with CVT, a vehicle with step-gear transmission has discrete gear ratios, which means that engine can not always work on the most efficient point. The optimal gear ratio and engine operation points are difficult to acquire, thus making the PnG for step-gear transmission hard to be applied.

The main contribution of this paper is to present a servo-loop PnG controller for road vehicles with step-gear transmission to pursue minimized fuel consumption in adaptive cruise control process. The main challenge lies in the fact that in a step-gear transmission, the gear ratio is discontinuous, which further leads to dispersed engine operating points. The servo-loop controller is designed based on a periodic switching map for the real-time implementation, and then is adjusted by a range-bounded feedback regulator to enhance the robustness to model mismatch. Compared to a conventional ACC controller, this design achieves up to 8.9% fuel reduction in naturalistic traffic flow when coasting at neutral gear in glide mode. The rest of this paper is organized as follows: Section 2 introduces the vehicle model for control; Section 3 explains the mechanism of open-loop PnG operation; Section 4 designs the servo-loop PnG controller, which is validated in Section 5; Section 6 concludes this paper.

II. Dynamic Car-following Model for Control

As shown in Fig. 1, this paper considers two consecutive vehicles in a typical car-following scenario: a preceding vehicle (PV), and a following vehicle (FV). The used FV is a passenger car with a gasoline engine, a 5-speed mechanical transmission, and a hydraulic braking system. The frontal-view radar is equipped for inter-vehicle range detection, and both gear position (i_g) and engine torque (T_e) are automatically controlled to fulfill the tracking task.

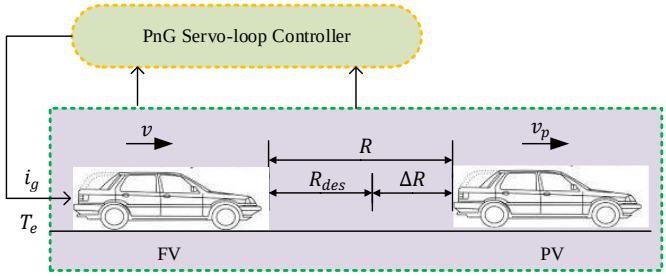

Fig. 1. A typical car-following scenario (R is the distance between FV and PV, v and v_p are the velocities of FV and PV).

The car-following dynamics is described by

$$\begin{aligned} \Delta\dot{v} &= a_p - a \\ \Delta\dot{R} &= \Delta v - \dot{R}_{des} \end{aligned} \tag{1}$$

where Δv is the relative speed, ΔR is the range error, a_p is the acceleration of PV, a is the acceleration of FV, R_{des} is the desired range between FV and PV, which follows a constant-time headway policy ($R_{des} = \tau_h v_p + d_0$) [29]. Considering the requirements of safety and traffic capacity, an inequality constraint is applied on the range error:

$$\Delta R_{min} \le \Delta R \le \Delta R_{max} \tag{2}$$

where ΔR_{min} and ΔR_{max} are the range error bounds, which can be set by drivers.

For the convenience of controller design, the powertrain dynamics of FV is simplified by assuming that: (1) FV runs on a flat and straight road, only having longitudinal motion; (2) The engine dynamics at intake manifold, chamber combustion, and fly wheels are lumped as a first order transfer function; (3) Such dynamics as tire slip and half-axle torsion are neglected; (4) The clutch engagement/disengagement and gear shifting are conducted instantaneously. In addition, no brake is assumed to be used in this paper for the purpose of minimizing energy dissipation in braking. The longitudinal dynamics of FV is described by

$$\begin{aligned} Ma &= -(C_A v^2 + Mgf) + \frac{\eta_T i_0}{r} T_e i_g(i) \\ i &\in [\mathrm{I}, \mathrm{II}, \mathrm{III}, \mathrm{IV}, \mathrm{V}] \end{aligned} \tag{3}$$

where M is the vehicle mass, C_A is the coefficient of aerodynamic drag, g is the gravity constant, f is the coefficient of rolling resistance, η_T is the mechanical efficiency of the

This article has been accepted for publication in a future issue of this journal, but has not been fully edited. Content may change prior to final publication. Citation information: DOI 10.1109/TVT.2016.2574740, IEEE Transactions on Vehicular Technology

driveline, T_e is the engine torque, $i_g(i)$ is the speed ratio of step-gear mechanical transmission, $i \in [\mathrm{I}, \mathrm{II}, \mathrm{III}, \mathrm{IV}, \mathrm{V}]$ is the five-level discontinuous gear position, i_0 is the main gear ratio and r is the radius of the wheels. The engine dynamics is described by a first-order transfer function:

$$T_e = \frac{1}{\tau_e s + 1} T_{ecom} \tag{4}$$

where T_{ecom} is the engine torque command, τ_e is the time constant of lumped engine dynamics. Saving fuel is the first priority of using the PnG operation, and therefore how to accurately calculate fuel consumption is critical to strategy design. For the studies in hybridized powertrain, static fuel maps are commonly used to predict engine fuel consumption [30], [31]. Simply using a static map, however, may generate significant errors due to transient dynamics of an engine. To account for the transient fuel consumption, a fuel model with correction term is used as

$$Q_s = q_{BSFC}(T_e, \omega_e) \cdot P_e + k_e \cdot \left(\frac{dT_e}{dt}\right)^2 \tag{5}$$

$$P_e = T_e \omega_e \tag{6}$$

where Q_s is the actual total fueling rate, q_{BSFC} is the static Brake Specific Fuel Consumption (BSFC) map, which is a tabular function of T_e (engine torque) and ω_e (engine speed), and k_e is the coefficient for transient fuel. The BSFC map of the engine used in this paper is shown in Fig. 2. The highly-nonlinear BSFC characteristics play an important role on determining fuel-minimized operation for road vehicles, which contains three types of lines (*i.e.*, optimal BSFC line, constant drive line, and engine drag line) and two critical points (minimum BSFC point, and idling point).

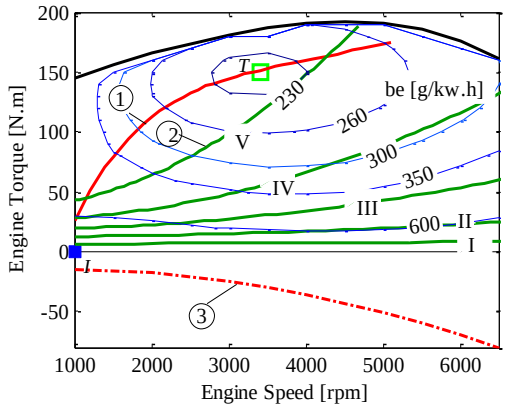

Fig. 2. The BSFC map of gasoline engine (Point T-minimum BSFC point, Point I- idling point; ①- optimal BSFC line; ②- constant drive line; ③- engine drag line).

In Fig. 2, optimal BSFC line actually has the highest operating efficiency for any given power. The engine drag line represents the engine operation at different speed when throttle is idling. The optimal BSFC line and engine drag line are fitted by using cubic polynomials:

$$T_{eBSFC} = \sum_{i=0}^{3} k_{eBSFC,i} \omega_e^i \tag{7}$$

$$T_{eDRAG} = \sum_{i=0}^{3} k_{eDRAG,i} \omega_e^i \tag{8}$$

where T_{eBSFC} is the engine torque at optimal BSFC line, T_{eDRAG} is the engine drag torque, $k_{eBSFC,i}$ and $k_{eDRAG,i}$ are the fitting coefficients. There are five constant drive lines, representing the engine operation points at each fixed gear position. The constant driving lines are calculated according to the simplified FV model (3) by assuming zero-acceleration:

$$T_{\mathrm{cs}}(i) = \left(C_A \left(\frac{\omega_e r_w}{i_0 i_g(i)}\right)^2 + Mgf\right) \frac{r_w}{\eta_T i_0} \frac{1}{i_g(i)} \tag{9}$$
$$i \in [\mathrm{I}, \mathrm{II}, \mathrm{III}, \mathrm{IV}, \mathrm{V}]$$

where $T_{\mathrm{cs}}(i)$ is the engine torque when constantly driving using gear i. Other vehicle parameters used for FV are listed in table I.

TABLE I
KEY PARAMETERS OF FV

Parameter	Value	Parameter	Value
M	$1600kg$	C_D	0.316
η_T	0.92	A_v	$2.22m^2$
r_w	$0.307m$	f	0.028
ρ_a	$1.29kg/m^3$	i_0	3.863
$i_g(i = \mathrm{I} \to \mathrm{V})$	$[3.620, 1.925, 1.285, 0.933, 0.692]$		

III. FUEL-SAVING MECHANISM OF OPEN-LOOP PNG

This section will discuss the fuel-saving mechanism of open-loop PnG operation. The explanation starts from the case of continuous variable transmission (CVT), which has continuous gear ratio, and then extends to the case of step-gear transmission, which only has finite number of discontinuous gear position. The mechanism analysis is of great importance to the design of servo-loop PnG control for ACC.

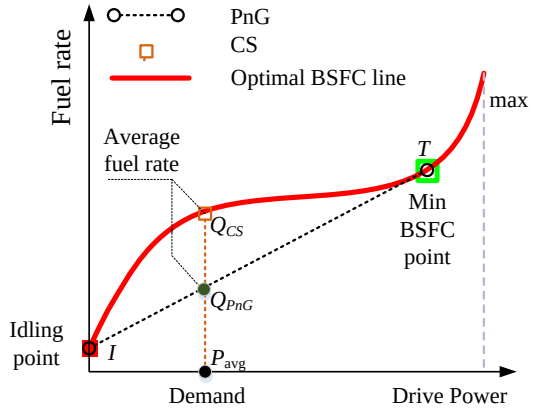

Fig. 3. The mechanism of PnG for CVT.

This article has been accepted for publication in a future issue of this journal, but has not been fully edited. Content may change prior to final publication. Citation information: DOI 10.1109/TVT.2016.2574740, IEEE Transactions on Vehicular Technology

A. *Open-loop PnG for continuous variable transmission*

For a powertrain with CVT, Li and Peng *et al*. (2012) have demonstrated that the PnG operation can achieve best fuel benefit in car-following scenarios. The PnG is an open-loop operating strategy, which first accelerates the vehicle to a higher speed by running engine at minimum BSFC point (called pulse mode or P mode, equivalent to operate at Point T in Fig. 2), and then idles the engine (called glide mode or G mode, equivalent to operate at Point I in Fig. 2) to coast down to a lower speed. Periodic switches between pulse mode and glide mode can achieve significant fuel benefit in car-following scenarios.

A graphic explanation has been proposed to exhibit the fuel-saving mechanism of PnG by Li and Peng *et al*. (2012) [23]. For idealized PnG, the CVT always regulates its speed ratio to enforce engine to work on optimal BSFC line, and therefore the fuel-saving feature of PnG actually origins from the S-shaped nonlinearity between engine fuel rate and engine power along optimal BSFC line. The S-shape nonlinearity actually first concaves up and then concaves down (as demonstrated in Fig. 3). Note that optimal BSFC line in Fig. 3 is a mapping from the $T_e - \omega_e$ coordinate in Fig. 2 to the $Q_s - P_e$ coordinate in Fig. 3 by considering (6). Compared to constant driving (with fuel rate fixed at Point Q_{cs}), a periodic switching operation between Point T and Point I has lower average fuel rate (Point Q_{PnG}) for any given power demand (Point P_{avg}).

B. *Open-loop PnG for step-gear transmission*

The abovementioned PnG strategy is exclusively suitable for CVT-based vehicles. This is because the speed ratio of CVT is continuous, which allows engine to be able to work along the optimal BSFC line. However, for step-gear transmission, the gear position becomes integer and limited in number. The discontinuous gear ratio can not ensure engine to exactly work at Point T on pulse mode and Point I on glide mode. Therefore, a PnG strategy needs to be adapted for step gear transmission in order to determine optimal engine torque and gear position. A new graphic explanation is proposed to explain the fuel saving mechanism for step-gear transmission. Interested readers can refer to Xu and Li *et al.* (2014) for detailed information [28].

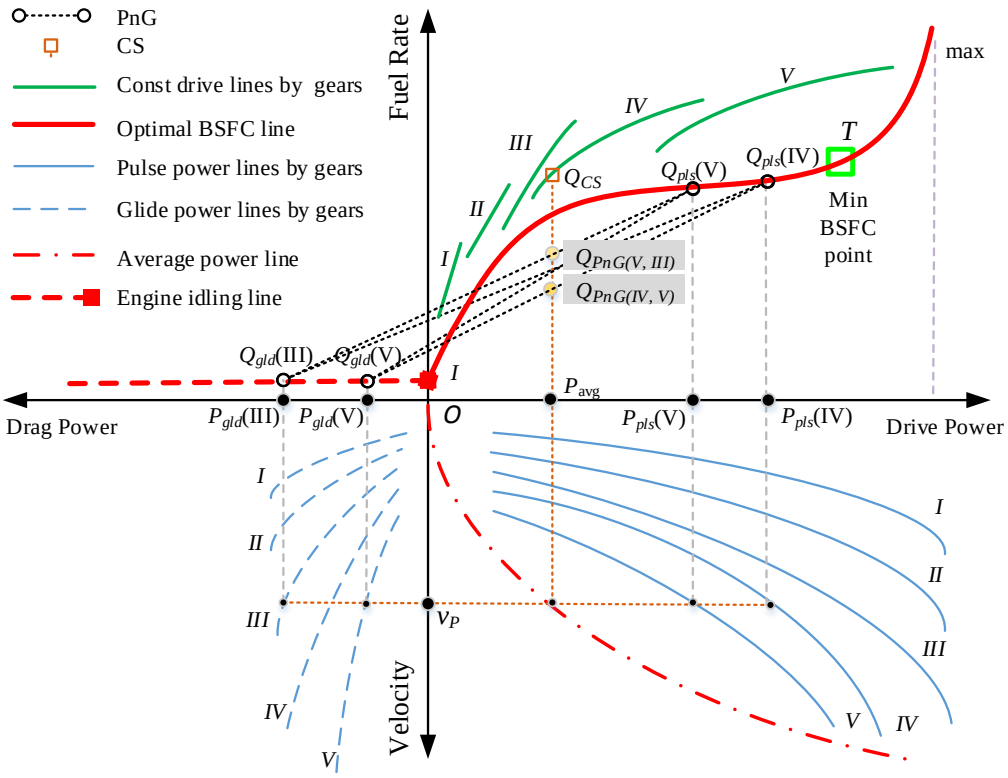

Fig. 4. The mechanism of PnG for step-gear transmission

The PnG for step-gear transmission can be explained by Fig. 4. Besides optimal BSFC line, Fig. 4 contains five other types of critical lines: average power line, pulse power line, glide power line, constant drive line, and engine idling line. The average power line describes the necessary power demand equal to the PV speed v_P:

$$P_{\text{avg}} = \frac{1}{\eta_T}\left(Mgfv_P + \frac{1}{2}C_{\text{D}}A_v\rho_{\text{a}}v_P^3\right) \tag{10}$$

where P_{avg} is the average power (Point P_{avg} in both Fig. 3 and Fig. 4). The pulse power line describes the necessary power under different gear position when engine is on pulse mode:

This article has been accepted for publication in a future issue of this journal, but has not been fully edited. Content may change prior to final publication. Citation information: DOI 10.1109/TVT.2016.2574740, IEEE Transactions on Vehicular Technology

$$P_{\text{pls}}(i) = \sum_{i=0}^{3} k_{eBSFC,i} \left(\frac{i_0}{r_w} v_P i_g(i) \right)^{i+1} \quad (11)$$
$$i \in [\text{I, II, III, IV, V}]$$

where $P_{\text{pls}}(i)$ is called pulse power. The glide power line describes the equivalent drag power at different gear position when engine is on glide mode:

$$P_{gld}(i) = \sum_{i=0}^{3} k_{eDRAG,i} \left(\frac{i_0}{r_w} v_P i_g(i) \right)^{i+1} \quad (12)$$
$$i \in [\text{I, II, III, IV, V}]$$

where $P_{gld}(i)$ is the drag power on glide mode. Similar to optimal BSFC line, both constant drive line and engine drag line in Fig. 4 are mappings from the $T_e - \omega_e$ coordinate (Fig. 2) to the $Q_s - P_e$ plot (Fig. 4) by considering (5) and (6). Note that engine idling line is assumed to be flat because engine consumes an approximately identical amount of fuel when idling (Equal to that at idling point I in Fig. 3).

The PnG for step-gear transmission still contains two modes: pulse mode (P mode) and glide mode (G mode). In the pulse mode, engine is regulated to work on optimal BSFC line by properly adjusting engine torque and gear position, while in the glide mode, engine is controlled to one of glide power lines. The best engine torque and gear position on two modes are determined by the following procedure according to Fig. 4.

TABLE II
THE OPTIMAL-TORQUE-OPTIMAL-GEAR (OTOG) ALGORITHM

For any given PV speed v_P,
- (1) Calculate average power P_{avg} using (10);
- (2) If using constant speed (CS) strategy:
  - (2.a) Find corresponding fuel rate Q_{CS} w.r.t. P_{avg} using constant drive lines;
  - (2.b) Determine desired gear position i_{comm} by which constant drive lines intersects with P_{avg}.
- (3) If using the PnG strategy:
  - (3.a) Calculate possible pulse power $P_{\text{pls}}(i)$ and glide power $P_{gld}(j)$ using (11) and (12) for $i, j \in [\text{I, II, III, IV, V}]$; Note that pulse or glide power might not exist because of engine physical limits and operating bounds.
  - (3.b) Find corresponding fuel rate points $Q_{pls}(i)$ for pulse mode w.r.t. $P_{\text{pls}}(i)$ using optimal BSFC line, and corresponding fuel rate points $Q_{gld}(j)$ for glide mode w.r.t. $P_{gld}(j)$ using idling line, for $i, j \in [\text{I, II, III, IV, V}]$;
  - (3.c) Find all candidate switching lines between pulse fuel rate points $Q_{pls}(i)$ and glide fuel rate points $Q_{gld}(j)$, noted as Line $i - j$, $i, j \in [\text{I, II, III, IV, V}]$; Each switching line represents one candidate periodic operation;
  - (3.d) Calculate the intersections between average power P_{avg} and candidate switching lines $i - j$, which are equal to the average fuel rate of candidate PnG operations, denoted as $Q_{PnG}(i, j)$;
  - (3.e) By minimizing $Q_{PnG}(i, j)$ to determine best gear ratios for pulse and glide at average PV speed v_P, i.e., $i_{g,pls}(v_P), i_{g,gld}(v_P)$. The corresponding optimal engine torque can be inversely computed by using optimal BSFC line and engine drag line, noted as $T_{eBSFC}(v_P), T_{eDRAG}(v_P)$.

C. Further discussion of open PnG

In short, a PnG always has two modes, i.e., pulse and glide. The pulse mode let engine work along optimal BSFC line as close as possible by properly selecting engine torque and gear position, which is relatively fixed. Unlike the pulse mode, the glide mode can have different selections due to some practical considerations, which leads to four types of PnG variants (demonstrated in Fig. 5).

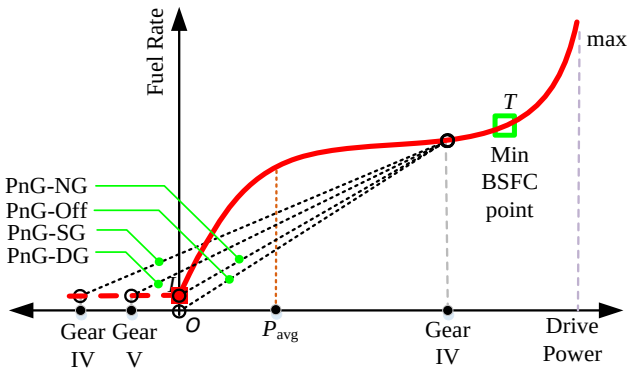

Fig. 5. Concept of four types of PnG variants

(V1) *Glide by using different but optimal gear position* (shorted as PnG-DG): The PnG-DG is actually the same PnG stated in Fig. 4, which allows to coast in gears. The optimal gear in coasting is given by the OTOG algorithm. It is easy to find that higher gear leads to lower fuel consumption, which is consistent with common experience of drivers, *i.e.*, higher gear position leads to lower engine speed and further smaller engine drag power.

(V2) *Glide by holding same gear to pulse* (shorted as PnG-SG): The PnG-DG causes frequent gear switching when mode changes, decreasing ride comfort and powertrain longevity. The PnG-SG is to fix the same gear in glide mode as that of pulse mode. This variant somewhat decrease fuel efficiency of PnG, but contributes to ride comfort and powertrain longevity.

(V3) *Glide with neutral gear and engine idling* (shorted as PnG-NG): To further improve fuel efficiency, another variant to select is neutral gear when gliding, which enforces $P_{gld} = 0$ by cutting off the power transmission from engine to wheels. This variant is equivalent to making engine work at Point I (Fig. 3), which leads to lower average fuel rate than both PnG-SG and PnG-NG.

(V4) *Glide with neutral gear and engine off* (shorted as PnG-Off): For any pulse operation, a line ending with Point O (original point) always has the lowest average fuel rate. This variant is equivalent to gliding with neutral gear and engine off,

This article has been accepted for publication in a future issue of this journal, but has not been fully edited. Content may change prior to final publication. Citation information: DOI 10.1109/TVT.2016.2574740, IEEE Transactions on Vehicular Technology

which means that no fuel is consumed in coasting. While having the best fuel efficiency, it is rather harmful to engine longevity due to frequent engine on-offs. Moreover, many engines might not support frequent automatic stop-and-start, which limits its practical usage.

IV. Design of Servo-Loop PnG Controller for ACC

The open-loop PnG is significantly beneficial to fuel economy. When applying it to servo-loop control, however, the powertrain dynamics will delay the mode switching and cause the overshoot in range error control. The existence of model uncertainties also has negative impact on the PnG control. All of these problems should be taken into consideration in the real-time implementation. The servo-loop PnG controller has to satisfying the following requirements:

(a) Engine periodically works on two modes, *i.e.*, pulse (P) and glide (G), by properly selecting gear position and engine torque. This periodic operation yields minimum fuel consumption for a given engine power.

(b) The FV automatically follows PV according to constant time-headway policy with range error bounded in a predefined range given by Eq. (2). This is the demand for adaptive cruise control system, which will fulfill car-following function.

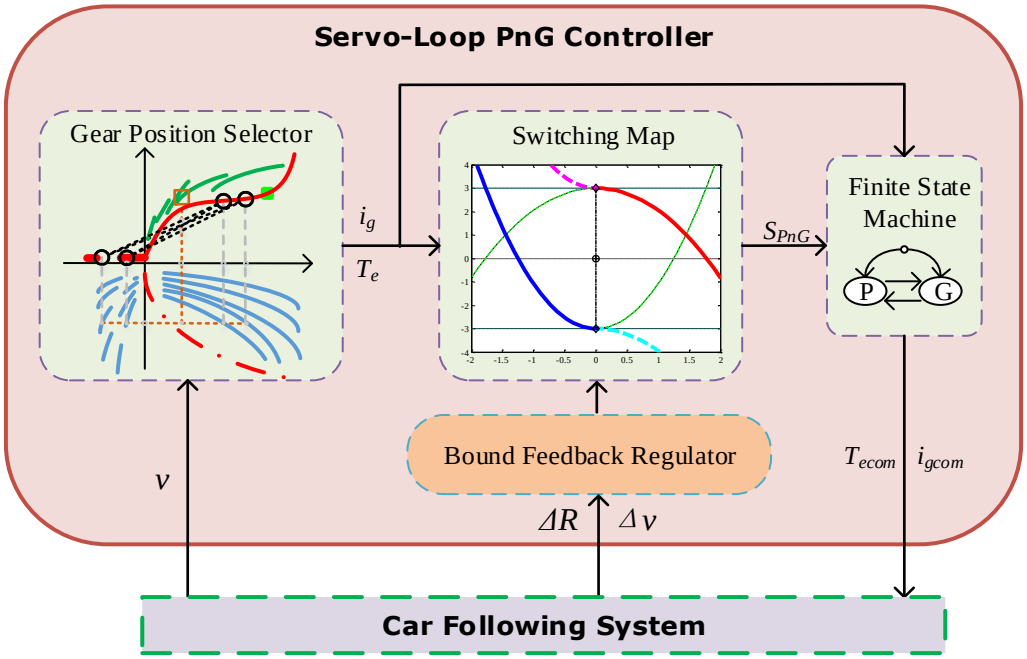

Fig. 6. Framework of the servo-loop PnG controller.

The configuration of servo-loop controller contains four main components: a gear position selector, a switching map, a finite state machine and a bound feedback regulator. The gear position selector is used to select the optimal gear position and engine torque in both P and G mode based on the OTOG algorithm. The switching map is crucial to servo-loop control by determining the used mode at current step, which will be discussed further in Section 4.2. The switching map generates a switching signal S_{PnG} $(P\ or\ G)$ to drive the finite-state machine. The finite state machine fulfills the mode switching and executes the commands of gear position and engine torque. The commands for FV are (Take PnG-DG as an example):

$$T_{ecom} = \begin{cases} T_{eBSFC}(v_P) & , \ if\ S_{PnG} = P \\ T_{eDRAG}(v_P) & , \ if\ S_{PnG} = G \end{cases}$$
$$i_{gcom} = \begin{cases} i_{g,pls}(v_P) & , \ if\ S_{PnG} = P \\ i_{g,gld}(v_P) & , \ if\ S_{PnG} = G \end{cases} \quad (13)$$

Note that other variants of PnG, i.e., PnG-SG, PnG-NG, PnG-Off, has different command when $S_{PnG} = G$. In reality, the unmodelled dynamics in powertrain and external disturbances from winds and roads could delay and distort the execution of commands, thus decreasing the car-following accuracy. The bound feedback regulator is used to correct driver desired range bound to maintain the accurate distance between FV and PV.

A. Initialization of PnG parameters

The initialization of PnG parameters include:

1) Select a PnG variant from PnG-DG, PnG-SG, PnG-NG. PnG-Off;
2) For any PV speed v_P, calculate the commands on engine torque and gear ratio, including $T_{eBSFC}(v_P)$, $T_{eDRAG}(v_P)$, $i_{g,pls}(v_P)$ and $i_{g,gld}(v_P)$, by using OTOG.
3) For any PV speed v_P, calculate the switching map according to Section 4.2.

B. Switching map for servo-loop control

The design of switching map is critical to the servo-loop controller, which relies on the fact that under the idealized PnG operation, the range error always reaches its bounds when the relative speed between PV and FV is zero [26]. For the idealized PnG operation, this section further assumes that (1)

This article has been accepted for publication in a future issue of this journal, but has not been fully edited. Content may change prior to final publication. Citation information: DOI 10.1109/TVT.2016.2574740, IEEE Transactions on Vehicular Technology

all dynamics in powertrain (including engine) are neglected; (2) the transmission efficiency under different gear ratio or different transmitted power is assumed being same; (3) The gear shifting is finished instantaneously, the influence of clutch is neglected; (4) PV runs at constant speed; and (5) the speed fluctuation in either pulse or glide mode is negligible. The switching map is drawn in the coordinating system of $(\Delta v, \Delta R)$. It contains two critical state trajectories, i.e., pulse switch line and glide switch line, which pass through the upper bound point $(\Delta v = 0, \Delta R = \Delta R_{max})$ and the lower bound point $(\Delta v = 0, \Delta R = \Delta R_{min})$, respectively. To mathematically describe these two critical trajectories, the FV acceleration on pulse and glide modes is needed

$$\begin{aligned}\bar{a}_{pls}(v_p) &= -\frac{C_A v_p^2 + Mgf}{M} \\ &\quad + \frac{\eta_T i_0}{M r_w} i_{g,pls} T_{eBSFC}, if\ Mode = P \\ \bar{a}_{gld}(v_p) &= -\frac{C_A v_p^2 + Mgf}{M} \\ &\quad + \frac{i_0}{M \eta_T r_w} i_{g,pls} T_{eDRAG}, if\ Mode = G\end{aligned} \tag{14}$$

Plugging (14) into (1), the relationships between $(\Delta v, \Delta R)$ could be derived as

$$\begin{aligned}\Delta v &= -\bar{a}_{pls}(v_p) t \\ \Delta R &= \Delta R_{max} - \frac{1}{2}\bar{a}_{pls}(v_p) t^2, \quad t \epsilon (-\infty, +\infty)\end{aligned} \tag{15}$$

$$\begin{aligned}\Delta v &= -\bar{a}_{gld}(v_p) t \\ \Delta R &= \Delta R_{min} - \frac{1}{2}\bar{a}_{gld}(v_p) t^2, \quad t \epsilon (-\infty, +\infty)\end{aligned} \tag{16}$$

The two critical trajectories divide the whole plot into three regions, i.e., pulse region, glide region and hold region. The location of state pair $(\Delta v, \Delta R)$ within different regions determines how to select S_{PnG}. Two state trajectories, the pulse switch line and glide switch line, could be calculated according to (15) and (16), as illustrated in Fig.7.

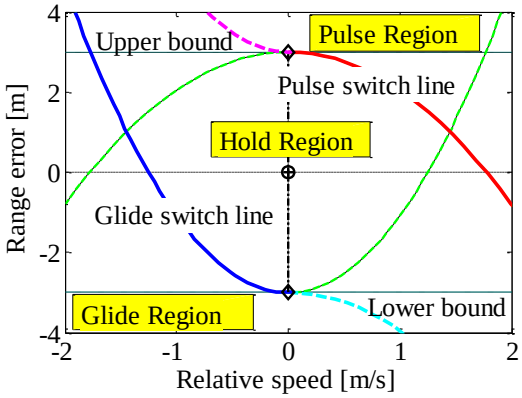

(a) Regional division by switch lines.

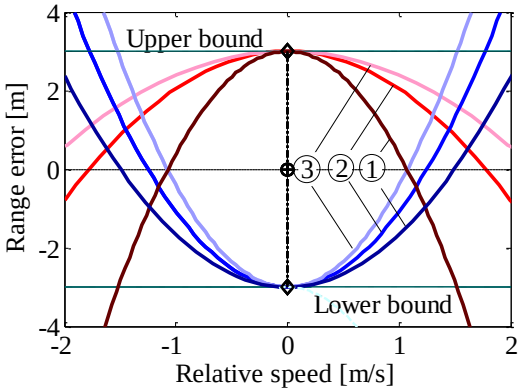

(b) Change of division with different v_P

Fig. 7. Concept of switching map. (①- switch lines of $v_P = 30m/s$; ②- switch lines of $v_P = 20m/s$; ③- switch lines of $v_P = 10m/s$)

In this study, $\bar{a}_{pls}$ and $\bar{a}_{gld}$ is not constant, but a function of the PV speed. Therefore, the switch and gliding lines in Fig. 7 (b) change their shapes as the PV speed varies. However, the two trajectories always pass the upper and lower bound points $(\Delta v = 0, \Delta R = \Delta R_{min}\ or\ \Delta R_{max})$, at which FV and PV have the same speed. In order to avoid frequent switching between P and G modes, a region-based switching logic is built

$$S_{PnG} = \begin{cases} P & if(\Delta v, \Delta R)\ \epsilon Pulse\ Region \\ S_{PnG}(n-1) & if(\Delta v, \Delta R)\ \epsilon Hold\ Region \\ G & if(\Delta v, \Delta R)\ \epsilon Gliding\ Region \end{cases} \tag{17}$$

Such a switching logic eventually forms a periodic PnG operation under the idealized conditions, driving the state $(\Delta v, \Delta R)$ to move counter-clockwise along the two trajectories. In reality, the speed fluctuation of FV will increase aerodynamic drag and the powertrain dynamics will bring time delay of driving operations to the response of vehicles. Therefore, a compensator is designed to correct the switching logic by considering real driving conditions. Interested readers can refer to [26] for more details.

C. *Range-bounded feedback regulator*

In reality, exogenous disturbances and parametric uncertainties inevitably exist in the car-following system, including road slope, environmental wind, uncertain vehicle mass, *et al*. As a result, the range constraint may be violated or unsatisfied, which will decrease the car-following smoothness and safety. To overcome their negative effect, a proportional feedback regulator for the bounds of range error is designed in this section. Take the upper bound regulator as an example, the upper bound error at k-th step is

$$e_{max}(k) = \varepsilon_{max}(k) - \Delta R_{max} \tag{18}$$

where ΔR_{max} is the desired upper bound initialized by drivers, $\varepsilon_{max}(k)$ is the maximum range error in reality. The virtual upper bound for next-step PnG operation is

$$\begin{aligned}\Delta \overline{R}_{max}(k+1) &= \Delta \overline{R}_{max}(k) - \lambda e_{max}(k) \\ 0 &< \lambda < 1\end{aligned} \tag{19}$$

This article has been accepted for publication in a future issue of this journal, but has not been fully edited. Content may change prior to final publication. Citation information: DOI 10.1109/TVT.2016.2574740, IEEE Transactions on Vehicular Technology

where $\Delta\overline{R}_{max}(k)$ is the virtual upper bound of k-th step and $\Delta\overline{R}_{max}(0) = \Delta R_{max}$ is the initial virtual upper bound. Similar feedback regulator can be designed for the lower bound of range error. The stability of the regulator is only proved for the idealized condition. First, we lump the effects of model uncertainties to the form of an error in longitudinal acceleration

$$\tilde{a}_{pls}(k) = \bar{a}_{pls}(k) + \varepsilon_a(k) \qquad (20)$$
$$|\varepsilon_a(k) - \check{\varepsilon}_a| \le \Delta\varepsilon_a$$

where $\bar{a}_{pls}(k)$ represents the pulse acceleration in the nominal case, $\tilde{a}_{pls}(k)$ denotes the pulse acceleration in the mismatch case, and $\varepsilon_a(k)$is the acceleration error due to the uncertainties. Note that $\varepsilon_a(k)$ is centered on $\check{\varepsilon}_a$, and the residue is bounded by $\Delta\varepsilon_a$, which actually presents the fluctuation of acceleration error. Fig. 8 shows the nominal and mismatch trajectories during one and a half PnG period.

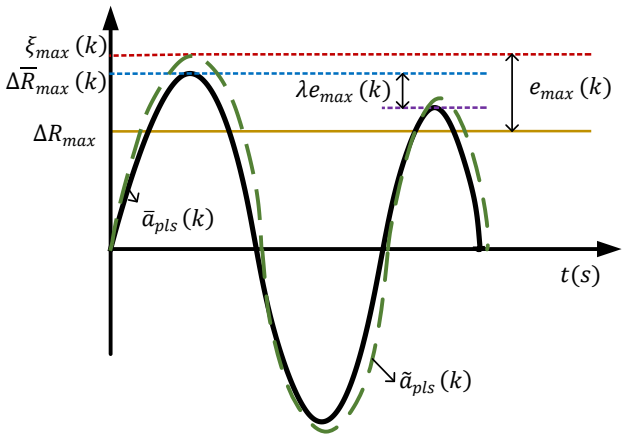

Fig. 8. Range bound feedback regulator

Using (15) in nominal and mismatch cases separately and canceling ΔR and t, we obtain

$$\Delta\overline{R}_{max}(k) = \xi_{max}(k) + \frac{\varepsilon_a(k)}{2\tilde{a}_{pls}(k)\bar{a}_{pls}(k)}\Delta\varepsilon_a^2 \qquad (21)$$

where $\xi_{max}(k)$ is the virtual bound in the mismatch case .

Combining (19), (20), and (21), we have the following inequality on $e_{max}(k)$ and its convergence property

$$\frac{e_{max}(k+1)}{e_{max}(k)} = 1 - \lambda + \frac{\varepsilon_a(k) - \varepsilon_a(k+1)}{2\tilde{a}_{pls}(k)\bar{a}_{pls}(k)e_{max}(k)}\Delta\varepsilon_a^2 \qquad (22)$$

$$\lim_{k\to\infty}|e_{max}(k)| = \frac{1}{\lambda}\frac{\Delta\varepsilon_a^3}{(a_{pls}(v_p) + \check{\varepsilon}_a(v_p))a_{pls}(v_p)} \qquad (23)$$

In a PnG, the PV speed v_p fluctuates, and $\Delta\varepsilon_a$ is the bound of the fluctuation of acceleration error. Although varied with different v_p, $a_{pls}(v_p)$ is always bounded at any given v_p due to the physical limit of engine. Therefore, $e_{max}(k)$ is bounded as k goes to infinity. Mathematically, $e_{max}(k) - e_{max}(k+1)$ has the same order of magnitude to $\Delta\varepsilon_a$. So, the third term of (22) is a third-order small quantities compared to the first two terms, which means that the third term could be neglected. Therefore $e_{max}(k)$ converges when $0 < \lambda < 1$ according to the Monotone Bounded Convergence Theorem. Besides, the larger λ is, the faster $e_{max}(k)$ converges.

V. Simulations and Analyses

The PnG controller introduced above is validated in two types of traffic flows, i.e., uniform traffic flow, in which the PV speed is constant; and naturalistic traffic flow, in which the PV speed profiles are extracted from a set of driver experiment data. For uniform traffic flow, every PnG variants (including PnG-DG, PnG-SG, PnG-NG, PnG-Off) are simulated with a speed step of 3m/s from 7m/s to 35m/s. As for the PnG control parameters, λ=0.5 is selected for the bound feedback regulator, ΔR_{max} = 3 m and ΔR_{max} = -3 m for the range bounds. A linear quadratic (LQ)-based controller is used as the benchmark. Its weighting matrices are selected to achieve a similar range error to that of the PnG controller.

A. Simulations in uniform traffic flow

In the uniform traffic flow, the PV speed is constant. Simulation results for v_P = 20 m/s are shown in Fig. 9.

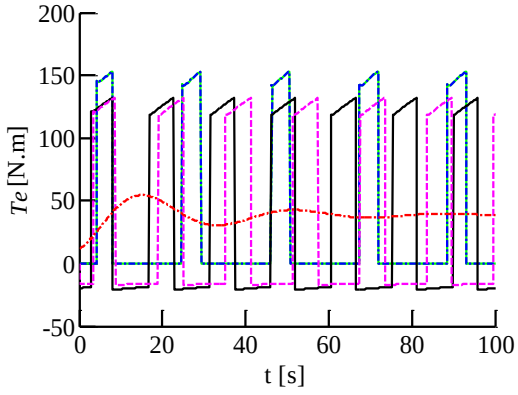

(a) Engine torque

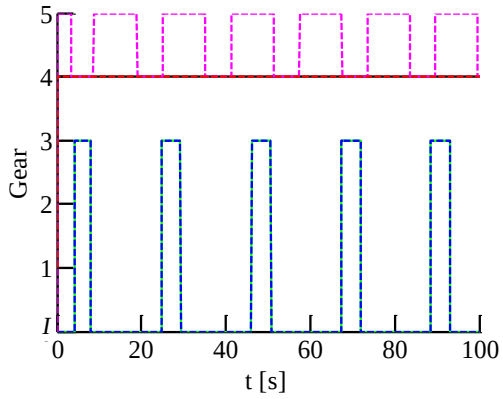

(b) Gear.

This article has been accepted for publication in a future issue of this journal, but has not been fully edited. Content may change prior to final publication. Citation information: DOI 10.1109/TVT.2016.2574740, IEEE Transactions on Vehicular Technology

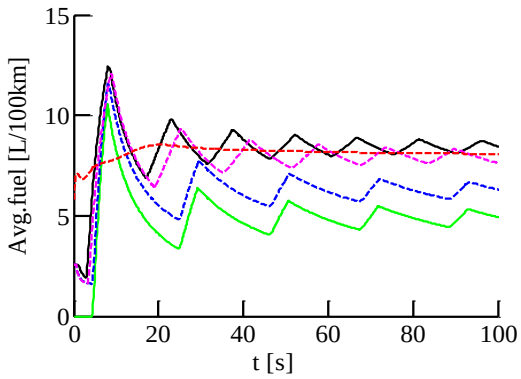

(c) Accumulated average fuel.

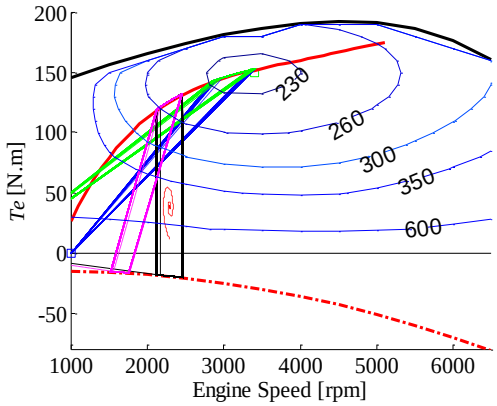

(d) Engine work points.

PnG-OFF PnG-NG PnG-SG PnG-DG LQ

Fig. 9. Performance under PnG and LQ controllers in a uniform traffic flow

Fig. 9 (a) shows that engine torque switch periodically between a high value and a low value. In the pulse phase, the engine torque operation points are around 147 N.m, which lie on the optimal BSFC line. In the glide phase, different PnG modes have different engine torque; for example, PnG-NG and PnG-Off have a constant value 0 N.m, PnG-SG's drag torque is about -24 N.m and the drag torque is around -20N.m for PnG-DG. It can be explained that lower gear ratio means lower engine speed under a certain vehicle speed, which results in a lower motored engine torque. It should be noted that the engine torque changes with engine speed in both pulse and glide phase due to the slightly increased or decreased vehicles speed.

The gear shift is shown in Fig. 9 (b). PnG-NG and PnG-Off switches between neutral gear and gear III, which is the optimal gear under this mode with a speed of 20 m/s. PnG-SG pulses and glides in a same gear IV, which is also the choice of LQ. PnG-DG switches between gear IV and gear V, which results in a lower drag torque compared to PnG-SG.

Fig. 9 (c) describes the average fuel consumption of four variants with v_P = 20 m/s. Fig. 9 (d) shows the engine operation points of the four variants. The engine works on the optimal BSFC line in pulse phase and on the drag torque line in the glide phase. In contrast, the LQ controller works at a low engine-efficiency points, which is the reason of the higher fuel consumption. In all, the fuel saving of different PnG variants at different speeds is shown in Fig. 10.

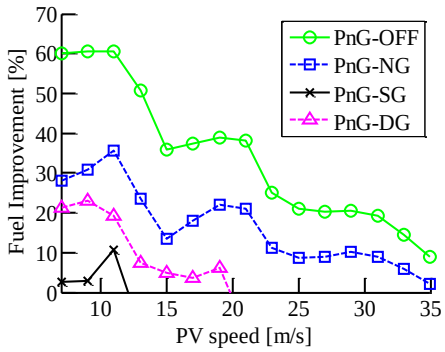

Fig. 10. Fuel improvement of PnG compared to LQ

It can be concluded that PnG-Off has the best fuel benefit. However, running the vehicles with engine off will do harm to safety and powertrain longevity. Therefore, PnG-Off might has no practical operability. Besides, PnG-NG has a relatively wide beneficial range in velocity (5-35 m/s). The benefit reaches its peak at 11m/s with the maximum saving up to 35.58% and then decreases to zero at 35 m/s, beyond which PnG is no longer beneficial. The benefit reaches to another crest at 19 m/s, which can be explained by the discontinuity of optimal gear position. PnG-SG and PnG-DG have poorer performances in both benefit range and fuel improvement compared to PnG-NG, which is consistent with the fact that the motored engine torque will cause more fuel consumption in glide phase. In addition, the function of bound feedback regulator is shown in Fig. 11.

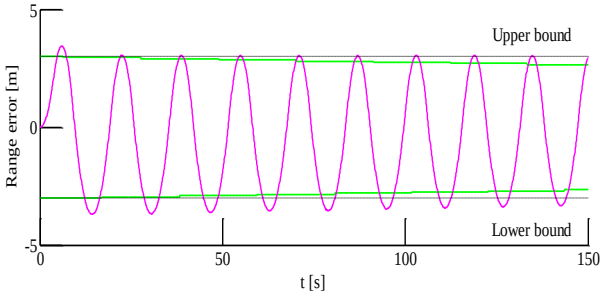

Fig. 11. Range error regulation of PnG controller

The setting upper and lower bound for PnG is 3 m and -3 m. It is shown in Fig. 11 that the range error is controlled to its initial bound after a few cycles of compensation due to the regulator.

B. Simulations in natural traffic flow

In the simulation of naturalistic traffic flow, the PV speed profile is obtained from a real vehicle test, which takes 10848s (around 3 hours) in total. Considering that ACC is often used at middle or high speed, we modified the speed profile by

This article has been accepted for publication in a future issue of this journal, but has not been fully edited. Content may change prior to final publication. Citation information: DOI 10.1109/TVT.2016.2574740, IEEE Transactions on Vehicular Technology

replacing the data points lower than 10 m/s with 10 m/s. The PV modified speed profile is shown in Fig. 12.

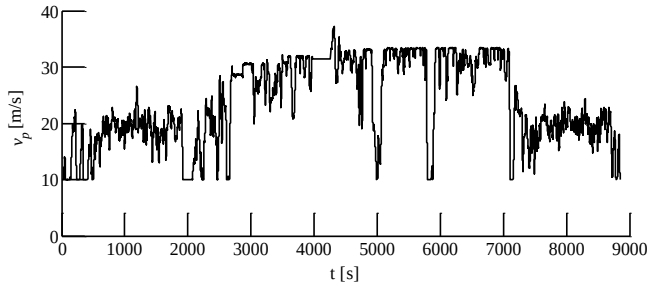

Fig. 12. Speed profile of actual driving data

The simulation results are shown in Fig. 13. (Only the results between 5200s and 5400s are shown in order to have a better view).

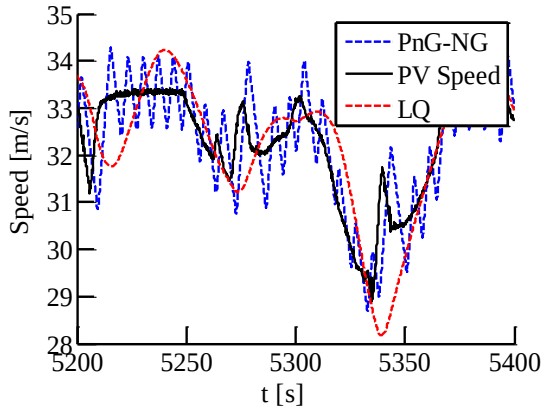

(a) Speed

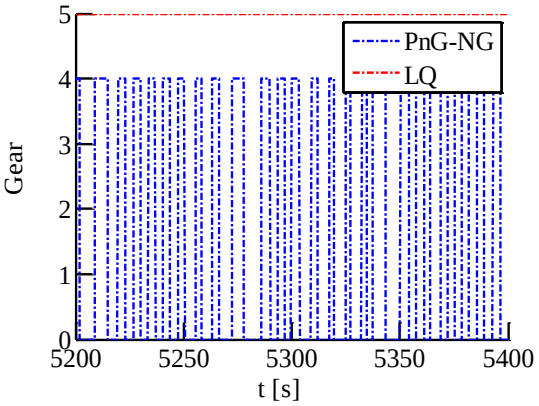

(b) Gear.

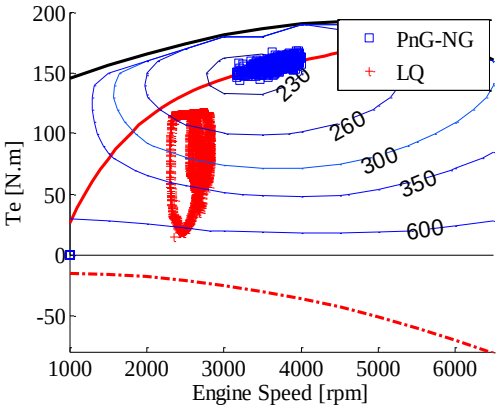

(c) Engine torque.

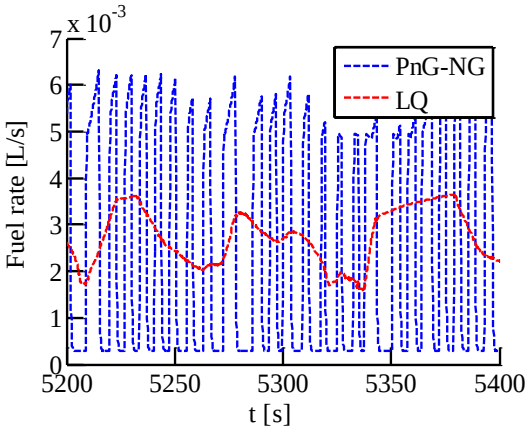

(d) Instantaneous fuel consumption.

Fig. 13. Performance under PnG-NG and LQ controllers in a natural traffic flow.

As shown in Fig. 13 (a), both PnG and LQ strategies have a relatively good speed-tracking effect. PnG-NG has a periodically speed feature while following the PV speed, and it maintains a relatively small speed fluctuation. LQ can generally track the PV speed but always has time delay and overshoot. Fig. 13 (b) shows the gear positions of PnG-NG and LQ. PnG-NG switches its gear between gear IV and neutral gear periodically and LQ works only on gear V during this section. Fig. 13 (c) shows that PnG-NG strategy always runs at BSFC line, and in contrast, LQ strategy works at other areas which have low efficiency. Fig. 13 (d) illustrates that PnG-NG has a periodically fuel injection rate but LQ has no regular feature. As a result, PnG-NG has a lower fuel consumption than LQ controller in natural traffic flow, which is consistent with the results of uniform traffic flow.

In order to have a deeper understanding of these two strategies, the frequency distributions of acceleration, speed error and range error under PnG and LQ controllers are shown in Fig. 14. As shown in Fig. 14 (a), the acceleration of PnG-NG shows a periodically feature, which is consistent with the analysis of gear and speed. In contrast, LQ has relatively small acceleration, since it mostly centered around 0 point, which means that LQ has a better performance on ride comfort. Fig. 14 (b) shows the speed error of the two strategies compared to PV speed. It can be summed up that PnG-NG has a relatively

This article has been accepted for publication in a future issue of this journal, but has not been fully edited. Content may change prior to final publication. Citation information: DOI 10.1109/TVT.2016.2574740, IEEE Transactions on Vehicular Technology

small speed fluctuation range. Fig. 14 (c) illustrates that both PnG-NG and LQ have an acceptable tracking effect, since their range error is bounded between -40m to 40m.

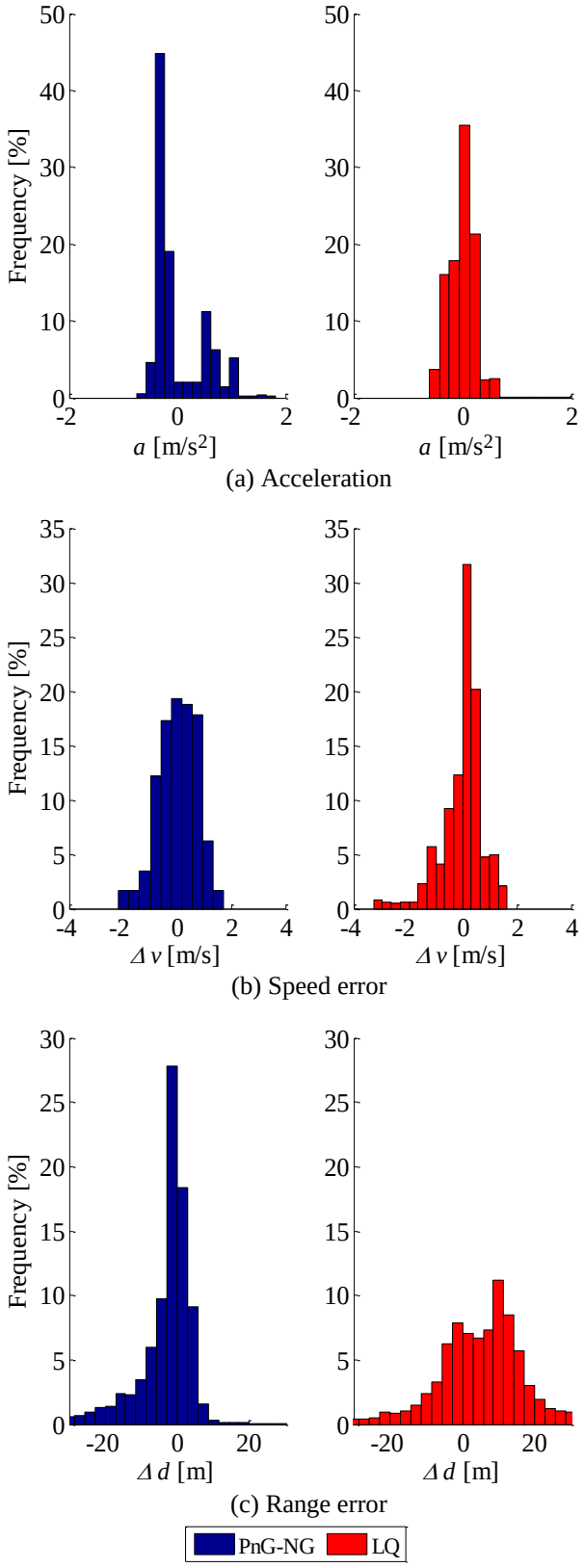

Fig. 14. Frequency distribution of acceleration, speed error and range error under PnG and LQ controllers

The fuel consumption of PnG-NG and LQ is shown in Fig. 15.

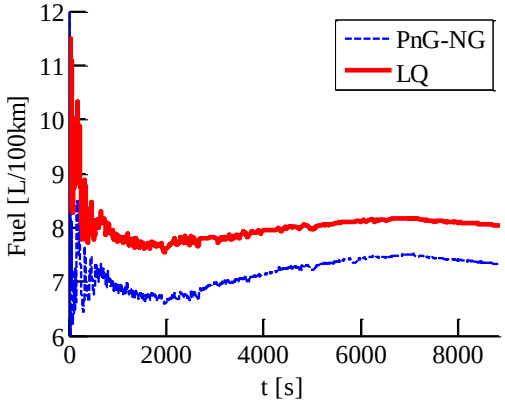

Fig. 15 Fuel consumption of PnG-NG and LQ in a naturalistic traffic flow

The fuel consumption of both PnG-NG and LQ fluctuates sharply at the beginning, because there is a lot of hard acceleration and deceleration during a relatively small time interval. As the simulation continues, fuel consumption tends to be stable. It is showed in Fig. 15 that PnG-NG has a lower fuel consumption compared to LQ. Using the total fuel consumption, we can find 8.9% fuel economy improvement of PnG-NG.

VI. Conclusions

This paper focuses on the mechanism and application of pulse-and-glide (PnG) strategy in road vehicles with step-gear transmission. A periodic servo-loop controller for adaptive cruise control system is designed and analyzed. The controller is also enhanced by a range-bounded feedback regulator to deal with model mismatch. Simulations under both uniform and naturalistic traffic flows were conducted to evaluate its fuel-saving performance. Simulation results in naturalistic traffic flow show that this servo-loop controller (when coasting at neutral gear) reduces fuel consumption by 8.9% compared to a benchmark LQ controller. Meanwhile, its inter-vehicle range is preferably bounded so that the negative impact on safety and traffic smoothness is contained.

In fact, the key to PnG strategy is the physical characteristics of vehicle's engine and transmission, originated from the S-shaped nonlinearity of engine fuel rate. Compared to the PnG under CVT, PnG under step gear transmission has four different variants: PnG-Off, PnG-NG, PnG-SG, and PnG-DG. PnG-Off has the best fuel-saving effect but lacks safety, due to which it should not be applied to practice. PnG-NG performs the best in the rest three variants while PnG-SG has the poorest effect. However, PnG-NG and PnG-DG require the vehicle to change gear positions periodically, which means that these two variants have a relative bad performance in ride comfort. All these features should be taken into account when applied to practice.

There are several ideal assumptions for both modeling and vehicle running conditions. For future works, assistant controllers should be built to overcome the negative influence of those factors when applying the PnG method into practice.

Besides, due to the switching nature of PnG, how to balance fuel benefit and NVH/comfort is important. From a long-term perspective, PnG might be implemented firstly on heavy-duty trucks. This is because there is more urgent need for fuel-saving techniques. In addition, the relatively low power/mass ratio means that the switching operations might be less perceptible. Furthermore, PnG might be widely used when automatic driving becomes matured in the near future, especially for commercial fleets.

REFERENCES

[1] S. Kobayashi, S. Plotkin, and S. K. Ribeiro, "Energy efficiency technologies for road vehicles," *Energy Efficiency*, 2(2), pp. 125-137, 2009.

[2] S. Kingham, J. Pearce, and P. Zawar-Reza, "Driven to injustice? Environmental justice and vehicle pollution in Christchurch, New Zealand," *Transportation Research Part D: Transport and Environment*, 12(4), pp. 254-263, 2007.

[3] H. J. Walnum and M. Simonsen, "Does driving behavior matter? An analysis of fuel consumption data from heavy-duty trucks," *Transportation research part D: Transport and Environment*, 3(6), pp. 107-120, 2015.

[4] C. Koffler and K. Rohde-Brandenburger, "On the calculation of fuel savings through lightweight design in automotive life cycle assessments," *The International Journal of Life Cycle Assessment*, 15(1), pp. 128-135, 2010.

[5] K. Fukuo, Koichi, A. Fujimura, M. Saito, K. Tsunoda, and S. Takiguchi, "Development of the ultra-low-fuel-consumption hybrid car–INSIGHT," *JSAE review*, 22(1), pp. 95-103, 2001.

[6] H. Zhang, J. Wang, and Y. Y. Wang, "Optimal Dosing and Sizing Optimization for a Ground Vehicle Diesel Engine Two-cell Selective Catalytic Reduction System," *IEEE Transactions on Vehicular Technology*, online available, 2016.

[7] H, Zhang and J. Wang, "Vehicle lateral dynamics control through AFS/DYC and robust gain-scheduling approach," *IEEE Transactions on Vehicular Technology*, 65(1), pp. 489-494, 2015.

[8] H. Zhang, G. Zhang, and J. Wang, "H-inf observer design for LPV systems with uncertain measurements on scheduling variables: application to an electric ground vehicle," IEEE/ASME Transactions on Mechatronics, online available, 2016.

[9] X. Hu, N. Murgovski, L. M. Johannesson, and B. Egardt, "Optimal dimensioning and power management of a fuel cell/battery hybrid bus via convex programming," *Mechatronics, IEEE/ASME Transactions*, 20(1), pp. 457-468, 2015.

[10] K. Boriboonsomsin, A. Vu, and M. Barth, "Eco-driving: pilot evaluation of driving behavior changes among US drivers," *University of California Transportation Center*, 2010.

[11] M. Sivak adn B. Schoettle, "Eco-driving: Strategic, tactical, and operational decisions of the driver that influence vehicle fuel economy," *Transport Policy*, 22, pp. 96-99, 2012.

[12] J. Van Mierlo, G. Maggetto, E. Van de Burgwal, and R Gense, "Driving style and traffic measures-influence on vehicle emissions and fuel consumption," *Proceedings of the Institution of Mechanical Engineers, Part D: Journal of Automobile Engineering*, 218(1), pp. 43-50, 2004.

[13] J. N. Barkenbus, "Eco-driving: An overlooked climate change initiative," *Energy Policy*, 38(2), pp. 762-769, 2010.

[14] B. Beusen, S. Broekx, T. Denys, C. Beckx, B. Degraeuwe, M. Gijsbers, K. Scheepers, L. Govaerts, R. Torfs, and L. Int Panis, "Using on-board logging devices to study the longer-term impact of an eco-driving course," *Transportation research part D: transport and environment*, 14(7), pp. 514–520, 2009.

[15] D. Barić, G. Zovak, and M. Periša, "Effects of eco-drive education on the reduction of fuel consumption and CO2 emissions," *PROMET-Traffic&Transportation*, 25(3), pp. 265-272, 2013.

[16] M. Zarkadoula, G. Zoidis, and E. Tritopoulou, "Training urban bus drivers to promote smart driving: A note on a Greek eco-driving pilot program," *Transportation Research Part D: Transport and Environment*, 12(6), pp. 449-451, 2007.

[17] F. Lattemann, K. Neiss, S. Terwen, and T. Connolly, "The predictive cruise control: A system to reduce fuel consumption of heavy duty trucks," *SAE transactions*, 113(2), pp. 139-146, 2004.

[18] E. Hellström, F. Anders, and L. Nielsen, "A real-time fuel-optimal cruise controller for heavy trucks using road topography information," SAE World Congress, pp. 1-8, 2006.

[19] E. Hellström, M.Ivarsson, J. Aslund, and L. Nielsen, "Look-ahead control for heavy trucks to minimize trip time and fuel consumption," *Control Engineering Practice*, 17.2, pp.245-254, 2009.

[20] S. Li, B. Yang, K. Li, H. Ukawa, D. Bai, and M. Handa, "A control strategy of ACC system considering fuel consumption," The 8th Inl. Symp. on Advanced Vehicle Control, Taipei, 2006.

[21] M. Hammache, M. Michaelian, and F. Browand, "Aerodynamic forces on truck models, including two trucks in tandem," SAE Technical Paper, No.: 2002-01-0530, 2002.

[22] S. Li, K. Li, R. Rajamani, and J. Wang, "Model predictive multi-objective vehicular adaptive cruise control," *IEEE Transactions on Control Systems Technology*, 19(3), pp. 556-566, 2011.

[23] S. Li, and H. Peng, "Strategies to minimize the fuel consumption of passenger cars during car-following scenarios," *Proceedings of the Institution of Mechanical Engineers, Part D: Journal of Automobile Engineering*, 226(3), pp. 419-429, 2012.

[24] S. Li, X. Hu, K. Li, and C. Ahn, "Mechanism of vehicular periodic operation for optimal fuel economy in free-driving scenarios," *IET Intelligent Transport Systems*, 9(3), pp. 306-313, 2014.

[25] J. Lee, "Vehicle inertia impact on fuel consumption of conventional and hybrid electric vehicles using acceleration and coast driving strategy," Diss. *Virginia Polytechnic Institute and State University*, 2009.

[26] S. Li, H. Peng, K. Li, and J. Wang, "Minimum fuel control strategy in automated car-following scenarios," *IEEE Transactions on Vehicular Technology*, 61(3), pp. 998-1007, 2012.

[27] S. Li, K. Deng, Y. Zheng, and H. Peng, "Effect of Pulse-and-Glide Strategy on Traffic Flow for a Platoon of Mixed Automated and Manually Driven Vehicles," *Computer-Aided Civil and Infrastructure Engineering*, 30(11), pp. 892-905, 2015.

[28] S. Xu, S. Li, X. Zhang, and B. Cheng, "Fuel-Optimal Cruising Strategy for Road Vehicles with Step-Gear Mechanical Transmission." *IEEE Transactions on Intelligent Transportation Systems*, 16(6), pp. 3496-3507, 2015

[29] P. Ioannou, and C. Chien, "Autonomous intelligent cruise control," *IEEE Transactions on Vehicular Technology*, 42(4), pp. 657-672, 1993.

[30] C. Lin, H. Peng, and J. Grizzle, "Power management strategy for a parallel hybrid electric truck," *IEEE Transactions on Control Systems Technology*, 11(6), pp. 839-849, 2003.

[31] Y. Yang, X. Hu, H. Pei, and Z. Peng, "Comparison of power-split and parallel hybrid powertrain architectures with a single electric machine: Dynamic programming approach," *Applied Energy*, 168, pp. 683-690, 2016.